Polarization singularities in 2D and 3D speckle fields

Florian Flossmann,[1] Kevin O'Holleran,[1] Mark R. Dennis,[2] and Miles J. Padgett[1]

[1]*Department of Physics and Astronomy, University of Glasgow, UK*
[2]*H. H. Wills Physics Laboratory, University of Bristol, Tyndall Avenue, Bristol BS8 1TL, UK*

The 3D structure of randomly polarized light fields is exemplified by its polarization singularities: lines along which the polarization is purely circular (C lines) and surfaces on which the polarization is linear (L surfaces). We visualize these polarization singularities experimentally in vector laser speckle fields, and in numerical simulations of random wave superpositions. Our results confirm previous analytical predictions (Opt. Commun. **213**, 201, 2002) regarding the statistical distribution of types of C points and relate their 2D properties to their 3D structure.

Topological defects play an important role in many physical phenomena [1], occurring in ordered media [2] and in propagating waves such as quantum wavefunctions [3] and, as we study here, light [4]. In scalar fields representing uniformly polarized optical beams, the defects are the widely studied optical phase singularities [4–6], also called nodes and optical vortices. Optical vortex lines in random 3D wave fields (speckle fields) were recently found to have Brownian scaling properties [7]. However, the most general optical beams also have position-dependent polarization, described by a complex vector field. In this case the singularities are places in the cross-section of pure circular or linear polarization. The resulting fields have many subtleties not present in the scalar case.

Within any transverse plane of a paraxial optical field it is useful to characterize the smoothly-varying polarization by streamlines oriented along the major axis of the polarization ellipse. Around every C point these streamlines rotate by $\pm\pi$, illustrated in Fig. 1 [8]. The positive index singularities occur in two forms: the *lemon* type, on which only one streamline terminates, and the less common *monstar*, on which three straight streamlines terminate. On negative-index singularities, termed *stars*, there are always three streamlines that terminate [9]. These singularities occur throughout polarization optics, e.g. tightly-focused beams and near-field optics [10], skylight [11] and crystal optics [12, 13]. As these fields propagate, the polarization changes continuously and the C points sweep out C lines.

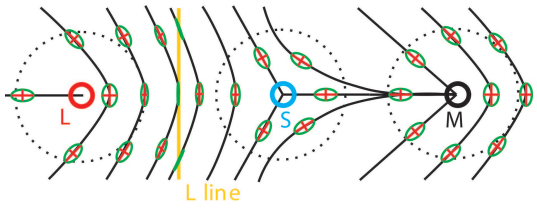

FIG. 1: In random vector fields C points are classified by the streamlines of their immediate surroundings into stars (S), monstars (M) and lemons (L). The polarizations may be either right- or left-handed, but C points of opposite handedness are always separated by an L line.

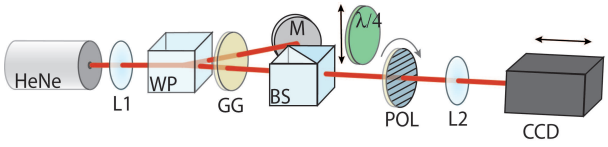

FIG. 2: Apparatus used to generate random vector speckle fields: HeNe laser incident on a Wollaston prism (WP) to doubly illuminate a ground glass screen. A polarizing beam splitter (BS) recombines the two beams. The transverse cross-sections immediately behind the ground glass screen were imaged with lens (L2) onto a 12-bit CCD camera mounted on a motorised stage.

In paraxial optical fields with random polarization (vector speckle fields), the field is dominated by its transverse components and the volume is filled with a complicated network of C lines, and surfaces of linear polarization (L surfaces) separating those of opposite handedness. These C lines are similar in their characteristics to the optical vortex lines encountered in the speckle patterns of scalar fields [7, 14]. Here, we establish the statistical frequency of stars, monstars and lemons, and compare our results to previous analytical predictions [9, 15].

In his seminal work [4, 8], Nye recognised that throughout the volume the C lines follow curved paths, exhibiting turning points and sometimes closed loops. At turning points the singularity's direction reverses with respect to the propagation direction, and its index changes sign. The singularity type therefore switches from star to lemon and vice versa, but near this transition the lemon singularity becomes a monstar. Away from these turning points, a lemon can switch to a monstar and back again.

The polarization state at each point of a light beam is completely described by the Stokes parameters (S_0, S_1, S_2, S_3) [16]. Operationally these parameters can be measured from the intensity of the light associated with different polarization states: S_0 is merely the overall intensity, and the others are given by

$$S_1 = I_{0^\circ} - I_{90^\circ},\ S_2 = I_{45^\circ} - I_{135^\circ},\ S_3 = I_{\text{left}} - I_{\text{right}}, \quad (1)$$

where I_θ is the intensity of the linear polarization at angle θ, and $I_{\text{left/right}}$ the intensity of the left/right circular polarization. L surfaces are those on which $S_3 = 0$ and

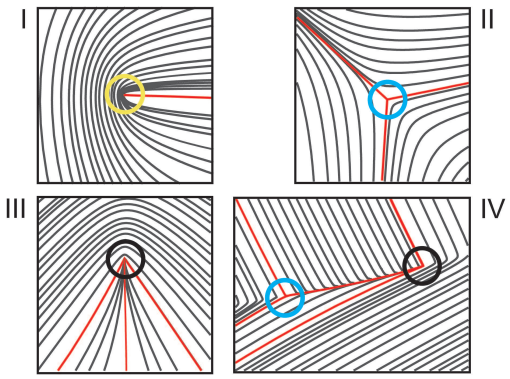

FIG. 3: Examples of four C points and nearby polarization streamlines as measured in our experiment. Part I is lemon type, part II star, part III monstar), and part IV a cross-section near a star-monstar transformation.

C lines are defined as the intercept of the loci $S_1 = 0$ and $S_2 = 0$. As described later, the type of C line singularity may be determined using the Stokes parameters.

In our experiment, illustrated in Fig. 2, the vector fields are generated by the interference of two orthogonally polarized speckle patterns created by illuminating two neighbouring regions of a ground glass screen with expanded beams derived from the same HeNe laser. The orthogonally polarized fields are superimposed using a polarizing beam splitter. A 12-bit CCD camera and imaging lens, mounted on a motorized stage, can be positioned to image any cross-section within the volume of interest [17]. The camera is preceded by a linear polarizer, which is rotated continuously as measurements are taken [18]. For any specific cross-section, the polarization at each point is obtained by acquiring a series of images as the polarizer undergoes one complete rotation. For one full rotation of the polarizer, every pixel in the image records a sinusoidal intensity modulation, which for elliptically polarized light contains a DC background. The Stokes parameters for each pixel can be calculated from this sinusoidal modulation. The overall intensity, S_0, is simply the average intensity, which is the first complex Fourier component, $\mathfrak{F}_1$. The eccentricity of the polarization ellipse can be found from the contrast of the sinusoidal modulation, whereas its direction is derived from the phase. Thus the second complex Fourier component, $\mathfrak{F}_2$, gives both S_1 and S_2,

$$S_0 = \sqrt{2/\pi}|\mathfrak{F}_1|, \qquad S_1 + iS_2 = 2\sqrt{2/\pi}\mathfrak{F}_2. \tag{2}$$

Inserting a $\lambda/4$-waveplate before the polarizer gives, after another full rotation of the polarizer, a different Fourier transform for each pixel, from whose second component $\mathfrak{F}_2^{\lambda/4}$, S_3 can be calculated:

$$S_3 = 2\sqrt{2/\pi}\mathrm{Im}(\mathfrak{F}_2^{\lambda/4}). \tag{3}$$

Determining the polarization in this way, based on many images, gives good measurement precision and a high degree of noise immunity. The process is automated and the Stokes parameters for every pixel in the cross-section can be found in approximately 10 seconds.

To accompany our measurements, we have numerically simulated vector speckle fields. These simulations are based on the superposition of two random scalar wave fields with opposite signs of circular polarization. Each of these fields is a superposition of about 3000 plane waves, randomly distributed in direction and with Gaussian distributed complex amplitudes. These amplitudes are subject to a Gaussian envelope to simulate the transverse power spectrum of laser light scattered from a rough surface [19]. The resulting interference is calculated over a large number of cross-sections to obtain the statistical distribution of stars, monstars and lemons. Calculating neighboring cross-sections creates a 3D structure of C lines and L surfaces. For all our simulations, we trial differing numbers of plane waves, differing fields of view and spatial resolution. As with our previous work on scalar fields [7], interference between a hundred plane waves, or more, repeatedly calculated over one or two coherence lengths, gives stable statistics for the singularities.

The data from the experiments and numerical simulation is a 3D grid of voxels, each having values for the four Stokes parameters. Noise is suppressed in the experimental data by filtering with a 3D Gaussian kernel. In every cross-section, the singularity index is calculated at each pixel from a line integral of the polarization angle, $\frac{1}{2}\arg(S_1 + iS_2)$. If this number is close to $\pm 1/2$ [8] the Stokes parameters S_1, S_2 are then interpolated to quadratic order and subjected to a zero-finding algorithm to locate the C point precisely. The singularity index of the C point is determined by the sign of D_I,

$$D_I = S_{1,x}S_{2,y} - S_{1,y}S_{2,x}, \tag{4}$$

where x, y subscripts denote spatial derivatives. If $D_I < 0$ then the singularity is a star, if $D_I > 0$ the singularity is a monstar or lemon. Monstars are then distinguished from lemons by the sign of D_L [15]:

$$\begin{aligned} D_L \;=\; & ((2S_{1,y} + S_{2,x})^2 - 3S_{2,y}(2S_{1,x} - S_{2,y})) \\ & \times((2S_{1,x} - S_{2,y})^2 + 3S_{2,x}(2S_{1,y} + S_{2,x})) \\ & -(2S_{1,x}S_{1,y} + S_{1,x}S_{2,x} - S_{1,y}S_{2,y} + 4S_{2,x}S_{2,y})^2. \end{aligned} \tag{5}$$

If three straight streamlines meet at the singularity then $D_L > 0$ and the singularity is a star or monstar, if $D_L < 0$ then the singularity is a lemon. Figure 3 shows the experimentally measured polarization streamlines in the vicinity of a number of C points.

A third classification, the contour classification, divides C points into hyperbolic or elliptic types [4]. This classification is related to the shape of contours of the polarization ellipse axis lengths, which form a double cone

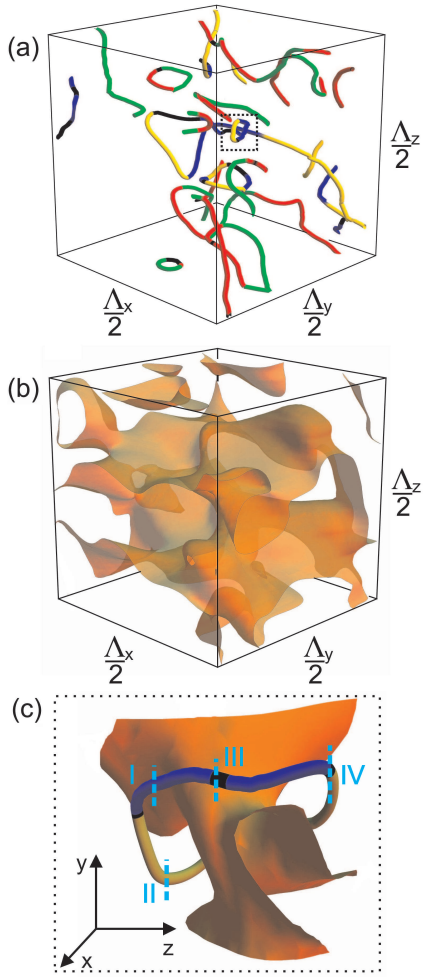

FIG. 4: Experimentally observed C lines (a) and associated L surfaces (b), where the (right/left handed) stars (green/blue) monstars (black) and lemons (red/yellow). (c) shows an expanded region of (a), highlighting a loop and the neighbouring L surface, the roman numerals highlighting cross-sections of interest, for which the streamlines are shown in Fig. 3.

structure near the singularity [4, 9, 20], and is an additional quantity which our observations determine. A C point is elliptic or hyperbolic depending on the sign of D_C, given by [15],

$$D_C = (S_{1,x}S_{2,y} - S_{1,y}S_{2,x})^2 - (S_{1,x}S_{0,y} - S_{1,y}S_{0,x})^2 - (S_{0,x}S_{2,y} - S_{0,y}S_{2,x})^2, \quad (6)$$

where $D_C < (>)0$ for hyperbolic (elliptic) C points.

The density of C points and the ratios of their different types in an isotropic random wave model were calculated in Ref. 15, based on earlier work by Berry and Hannay on umbilic points on random surfaces [9]. The density of C points per unit coherence area was calculated to be $4\pi\Lambda_T^{-2}$ (where Λ_T is the transverse coherence length of the complex vector field) and the star:lemon:monstar ratio is $50:44.72:5.28$. Since C points in random vector speckle fields are the vortices in the independent, identically distributed left and right circular components, the C point density is twice the underlying vortex density of $2\pi\Lambda_T^{-2}$ [14], which has been verified experimentally [21]. Polarization singularity densities have previously been investigated in experiments [22], but with data sets that were too small to give average densities. Table I shows the breakdown of observed and simulated C points into their singularity type, in the index/line classification (lemon, monstar or star) and contour classification (elliptic or hyperbolic). Our quoted errors are a combination of statistical uncertainty based on the finite numbers of singularities found and by varying the radius of the line integral around the C points. However, in all cases our agreement with the analytic statistics predictions [15] is excellent. Additionally, we find the density of numerically simulated C points is $12.51\Lambda_T^{-2}$, which is close to the predicted value of $4\pi\Lambda_T^{-2} \approx 12.57\Lambda_T^{-2}$.

Singularity type	simulation	experiment	Dennis[15]
Star	0.501 ± 0.002	0.506 ± 0.003	0.500
Lemon	0.450 ± 0.003	0.443 ± 0.002	0.447
Monstar	0.049 ± 0.002	0.050 ± 0.003	0.053
Star E/H	1.035 ± 0.054	1.073 ± 0.078	1.000
Lemon E/H	1.133 ± 0.078	1.086 ± 0.112	1.104
Monstar E/H	0.418 ± 0.056	0.487 ± 0.031	0.404

TABLE I: Fraction of C points of different types in transverse cross-sections and ratio of elliptic to hyperbolic types (E/H). The simulations average over > 90000 C points, the experiments over > 35000 C points.

In our previous numerical study of optical vortices in scalar speckle [7], we found that about 73% of the vortex length is in infinite lines, the remainder in closed loops. For lengthscales above the coherence length of the field, the vortex lines scale as fractals of dimension 2. Since random polarization fields (theoretically and experimentally) are superpositions of independent random fields in their left and right circular components – in which the C lines are vortices of the appropriate component – we conjecture that C lines in random vector speckle similarly scale like Brownian random walks. However, the C point type, being a vector property of the singularity, cannot be deduced from the underlying scalar field.

Figure 4 shows a typical experimental observation of the C line (a) and the associated L surface (b) structure within a random vector speckle field. They are plotted over a natural coherence volume $\Lambda^3 = \Lambda_T^2\Lambda_z$, where Λ_z is the longitudinal coherence length. The C lines are color coded to denote stars, monstars and lemons of both right and left handed circular polarization. As anticipated [4, 8], we note that points on C line loops are mainly stars and lemons, with short monstar sections at the maximum and minimum z-extent. Monstars also frequently occur within the lemon section of the C line, far away from the turning points, and it is these monstars that appear

Singularity type	simulation	experiment
Star	0.504 ± 0.008	0.496 ± 0.011
Lemon	0.420 ± 0.005	0.422 ± 0.010
Monstar	0.076 ± 0.005	0.082 ± 0.011
Star E/H	0.814 ± 0.039	0.727 ± 0.081
Lemon E/H	0.944 ± 0.058	0.787 ± 0.010
Monstar E/H	0.260 ± 0.028	0.274 ± 0.038

TABLE II: Fraction of C lines of different type and ratio of elliptic to hyperbolic (E/H) types, evaluated over numerically simulated ($5 \times \Lambda^3$) and experimentally observed ($2 \times 1.25\Lambda^3$) volumes.

most common. Figure 4 (c) shows a small section of the same volume highlighting one C line loop and the linearly polarized L surface in its vicinity, separating it from the C lines of opposite handedness. Sections I-IV are those for which the streamlines are plotted in Fig. 3.

By rescaling z, so the coherence lengths $\Lambda_T = \Lambda_z = \Lambda$, we expect the tangent direction of C lines to be uniformly distributed. From the solution to the classical 'Buffon needle problem' [23], generalized to lines in 3D [24], the C line density per unit coherence volume ought to be twice the C point density in transverse section, i.e. $8\pi\Lambda^{-2} \approx 25.133\Lambda^{-2}$. Our numerical simulations give this line density as $25.76\Lambda^{-2}$.

We also consider the distribution of singularity type as a fraction of C line length, given in Table II. These are different from the results of Table I, where the density is weighted in proportion to the z-component of the C line tangent. In particular, since monstars occur when C lines are approximately perpendicular to the propagation direction, their 3D weighting is higher (7.6%) than in transverse sections (5.3%). It appears also that the elliptic weighting dominates over the hyperbolic. As yet there are no analytic calculations for these numbers to match the results of Table II, although for fields where the polarization ellipse plane orientation is also random [25], we expect the 3D weightings to match Table I.

In conclusion, we have experimentally visualized polarization singularities – C lines and L surfaces – in random vector speckle fields. We reasoned that the large scale structure is identical to that recently reported for vortices in scalar speckle fields. In addition to verifying the singularity type distribution in 2D against theoretical predictions, we have new experimental and simulated predictions for their three-dimensional counterparts, including through the Buffon needle problem a link between their 2D and 3D statistics.

This work was supported by the Leverhume Trust and FF by the Deutsche Forschungsgemeinschaft (DFG). MRD is supported by the Royal Society.

[1] N. D. Mermin, Rev. Mod. Phys. **51**, 591 (1979).
[2] D. R. Nelson *Defects and geometry in condensed mater physics*, Cambridge University Press, Cambridge (2002).
[3] P. A. M.Dirac *Proc. R. Soc. Lond. A* **133**, 60 (1931).
[4] J. F. Nye, *Natural focusing and fine structure of light*, Institute of Physics Publishing, Bristol (1999).
[5] A. S. Desyatnikov, Y. S. Kivshar and L. Torner Prog. Opt **47**, 291 (2005).
[6] L. Allen, M. J. Padgett and M. Babiker Prog. Opt **39**, 291 (1999).
[7] K. O'Holleran, M. R. Dennis, F. Flossmann and M. J. Padgett *Phys. Rev. Lett.* **100**, 053902 (2008).
[8] J. F. Nye, *Proc. R. Soc. Lond. A* **389**, 279 (1983).
[9] M. V. Berry and J. H. Hannay, *J. Phys. A* **10**, 2083 (1977).
[10] K. Lindfors, A. Priimagi, T. Setala, *et al.* Nature Photonics **1**, 228 (2007).
[11] M. V. Berry, M. R Dennis, and R. L. Lee, *New J. Phys.* **6**, 162 (2004).
[12] F. Flossmann, U. T. Schwarz, M. Maier and M. R. Dennis *Phys. Rev. Lett.* **95**, 253901 (2005).
[13] F. Flossmann, U. T. Schwarz, M. Maier and M. R. Dennis *Opt. Express* **14**, 11402 (2006).
[14] M. V. Berry and M. R. Dennis, *Proc. R. Soc. Lond. A* **456**, 2059 (2000).
[15] M. R. Dennis, *Opt. Commun.* **213** 201 (2002).
[16] M. Born and E. Wolf, *Principles of Optics*, Pergamon Ress Oxford, (1959).
[17] K. O'Holleran, M. J. Padgett and M. R. Dennis *Opt. Express* **14**, 3039 (2006).
[18] J. S. Tyo, D. L. Goldstein, D. B. Chenault and J. A Shaw *Appl. Opt.* **45**, 5453 (2006).
[19] J. W. Goodman, *Speckle Phenomena in Optics*, Ben Roberts and Co. (2006).
[20] R. I. Egorov, M. S. Soskin and I. Freund *Opt. Lett.* **31**, 2048 (2006).
[21] W. Wang, S. G. Hanson, Y. Miyamoto and M. Takeda *Phys. Rev. Lett..* **94**, 103902 (2005).
[22] V. G. Denisenko, R. I. Egorov and M. S. Soskin *JETP Lett.* **80**, 17 (2004).
[23] M. Aigner and G. M. Ziegler *Proofs from THE BOOK*, Springer (2001).
[24] M. R. Dennis *Eur. Phys. J. Special Topics* **145**, 191 (2007).
[25] M. V. Berry and M. R. Dennis, *Proc. R. Soc. Lond. A* **457**, 141 (2001).